Developing novel potent Anti-Histamine H1 receptor antagonists: A DFT Study

Senthilkumar T
[1]Assistant Professor, Department of Chemistry, P.B. College of Engineering, Irungattukottai, Sriperumbudur Taluk, Chennai, Tamil Nadu-602117

[3]Research Scholar, Department of Chemistry
Kongunadu Arts and Science College, Coimbatore, Tamilnadu, India-641 029

Dr. V.D. Nadhiya[2]
Assistant Professor, Department of Physics
Kongunadu Arts and Science College, Coimbatore, Tamilnadu, India-641 029

Dr. A. Manimaran[3]
Assistant Professor, Department of Chemistry
Kongunadu Arts and Science College, Coimbatore, Tamilnadu, India-641 029

Dr. K. Saminathan[3, *]
Assistant Professor, Department of Chemistry
Kongunadu Arts and Science College, Coimbatore, Tamilnadu, India-641 029.

Abstract : **A structure investigations of Brompheniramine or Dexbrompheniramine maleate viz., the geometry structure optimization, frequencies (IR), NMR, electronic character, frontier molecular orbital (HOMO-LUMO) and first static hyperpolarizability (β_{tot}) studies of reportedcompound were calculated using DFT with B3LYP/6-311G(d,p) level of theory in gas phase and DMSO solvent. The calculated HOMO and LUMO energies showed that charge transfer occurs within the molecule and from the molecular electrostatic potential (MEP), the molecular stability and bond strength have been explained. In addition to that to find the influence of energy gap (ΔE_{gap}) between the HOMO-LUMO orbitals on the first static hyperpolarizability (β_{tot}), was calculated the ΔE_{gap} for all theBrompheniramine compound and the results revealed that the smaller HOMO-LUMO ΔE_{gap} is, larger be the β_{tot} is.**

Keywords – Brompheniramine, DFT, HOMO-LUMO, MEP, (ΔE_{gap}), first static hyperpolarizability (β_{tot})

I. INTRODUCTION

Histamine predominates in a series of physiological processes, like in the functions of immune cells, gastrointestinal tract and CNS (central nervous system). For instance, histamine in CNS is closely connected with a wide spectrum of functions, like the regulation of arousal and the sleep-wake cycle, appetite control, satiation, nociception and cognition [1]. Antihistamines were first introduced in the 1940s and represent one of the most commonly-used medications today [2]. This is just due to the specific histamine-blocking capability and marked sedative effects; H1-antihistamines are often used for sleep promotion nowadays [3]. Meanwhile, in quite a few medications, anti-histamines are also applied for the treatment of allergies, cold symptoms, nausea, itching and insomnia. However, after bedtime use of anti-histamines, the long plasma half-lives and protracted CNS exposure always are assumed to cause the frequently-occurring next-day impairment, which in turn suggests the importance of an improved pharmacokinetic profile in the selection of new insomnia-aimed H1-antihistamines [4]. As a result, for the treatment of insomnia, the use of novel and selective H1-antihistamines with appropriate exposure is promising as an alternative to current medications, especially for sleeping improvements during the latter third of the night and overall sleep efficiency [5]. Such agents increase sleep time and improve sleep efficiency [6].

As a matter of fact, the development of H1-antihistamines has undergone three generations. The first-generation antihistamines, which are also known as sedative antihistamines, contain brompheniramine, chlorphenamine and mepyramine (an ethylenediamine), hydroxyzine (a piperazine), diphenhydramine (an ethanolamine), promethazine (a phenothiazine) and triprolidine (alkylamine derivative) [7].

However, the side effects are obvious for the first-generation H1-antihistamines:

- because of their poor receptor selectivity and high penetration rate of the blood-brain barrier, a depression of the CNS appears, which always leads to many symptoms, like not only drowsiness, fatigue, somnolence and dizziness, but also impairments of cognitive function, memory and psychomotor performance;
- cardiac problems also appear due to anti-muscarinic effects, blockade of cardiac ion currents and α-adrenergic-receptor blockade
- other problems occur owing to the ability to block α-adrenergic, muscarinic and serotoninergic receptors, which in turn bring about dry eyes, dry mouth, mydriasis, urinary retention, constipation, erectile dysfunction, gastrointestinal motility and memory deficits [8].

Computational drug discovery and optimization approaches, based on quantitative structure-activity alternative for drug development when employed in conjunction with synthetic alternative for drug development when employed in conjunction with synthetic medicinal chemistry and experimental testing of lead compounds [9-12].

The rest of the paper is organized as follows. Proposed computational investigation is explained in section II. Experimental results are presented in section III. Concluding remarks are given in section IV.

II. COMPUTATIONAL INVESTIGATION

2.1. DFT Calculations

The Brompheniramine or Dexbrompheniramine maleate [9-12] derivatives (Scheme 1) have active pyridine moety which is most polarizable, the DFT study is vital to determine the structural parameters in accuracy with B3LYP/6-311G(d,p) level theory and quantum mechanical investigations have been computed with the GAUSSIAN 09W program package [13-18]. The program used to optimize structures, and calculate PES, vibrational frequencies (IR), electronic transition, TD-DFT and gauge-including atomic orbitals (GIAOs) to calculate NMR shielding tensors (^{13}C and ^{1}H) [19-22].

The Mulliken Charges, APT charges, the energies of the frontier molecular orbitals (HOMO/LUMO) with molecular energy level diagram, electrostatic potential surface and Laplacian electron density analysis and molecular first static hyperpolarizability (β_{tot}) were also computed [22-26].

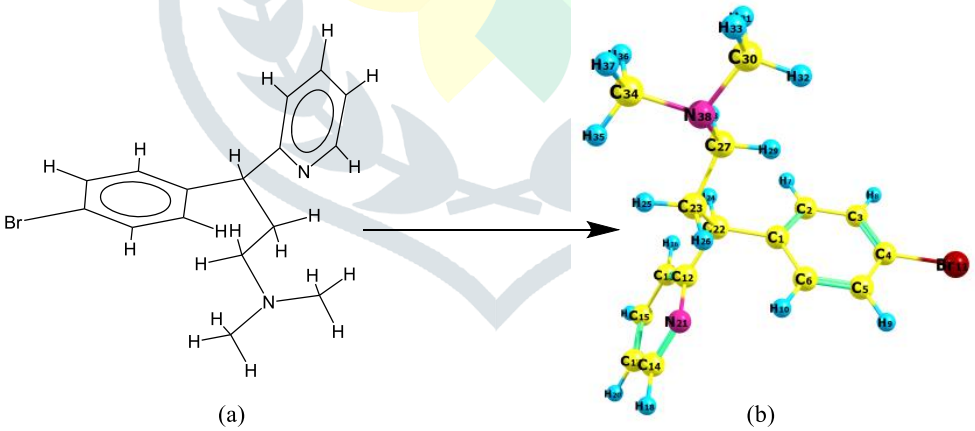

Figure 1. (a) Structure of Brompheniramine or Dexbrompheniramine maleate (AHC1); (b) Optmized structure of (AHC1) using DFT-B3LYP/6-311G (d,p)

The GaussView 6.0.16 visualization programme [27] and Chemcraft version 1.8 have been employed to generate the Laplacian electron density maps, HOMO-LUMO and ESP contour surfaces.

III. RESULTS AND DISCUSSION

3.1. Geometry Optimization

The optimized structures of the Brompheniramine or Dexbrompheniramine maleate (AHC1) shown (Figure 1) and it potential energy surface diagram (PES) (Figure 2) with numbering the atoms and geometry optimizations of the title compound was computed without symmetry constraints of C-C and C-H bond lengths and bond angles [15].

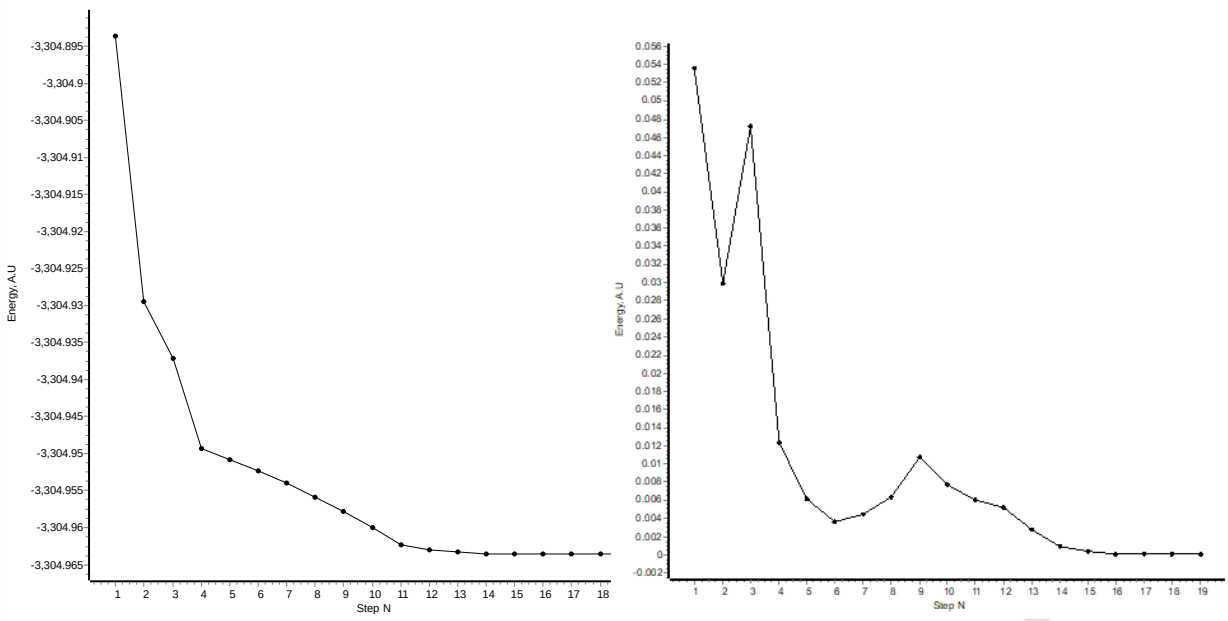

(a) (b)

Figure 2. PES Diagram of AHC1 ((a) Energy vs Steps and (b) Optimization Convergence)

Table 1. Computed bond length parameters of AHC1

S.No.	Atoms	Bond Length (Å)
1.	N(38)-C(27)	1.463
2.	N(38)-C(34)	1.457
3.	N(38)-C(30)	1.457
4.	H(37)-C(34)	1.093
5.	H(36)-C(34)	1.108
6.	H(35)-C(34)	1.091
7.	H(33)-C(30)	1.093
8.	H(32)-C(30)	1.093
9.	H(31)-C(30)	1.107
10.	H(29)-C(27)	1.093
11.	H(28)-C(27)	1.110
12.	C(27)-C(23)	1.531
13.	H(26)-C(23)	1.092
14.	H(25)-C(23)	1.094
15.	H(24)-C(22)	1.095
16.	C(23)-C(22)	1.547
17.	C(22)-C(12)	1.525
18.	C(22)-C(1)	1.527
19.	N(21)-C(14)	1.335
20.	N(21)-C(12)	1.340
21.	H(20)-C(17)	1.083
22.	H(19)-C(15)	1.084
23.	H(18)-C(14)	1.087
24.	C(17)-C(15)	1.391
25.	C(17)-C(14)	1.392
26.	H(16)-C(13)	1.084
27.	C(15)-C(13)	1.390
28.	C(13)-C(12)	1.399
29.	Br(11)-C(4)	1.921
30.	H(10)-C(6)	1.083
31.	H(9)-C(5)	1.082
32.	H(8)-C(3)	1.082
33.	H(7)-C(2)	1.085
34.	C(6)-C(1)	1.400
35.	C(6)-C(5)	1.392
36.	C(5)-C(4)	1.392
37.	C(4)-C(3)	1.389
38.	C(3)-C(2)	1.394
39.	C(2)-C(1)	1.397

Table 2. Computed Bond angle parameters of AHC1

S.No.	Atoms	Bond Angle (Å)
1.	C(30)-N(38)-C(34)	110.786
2.	C(30)-N(38)-C(27)	111.437
3.	C(34)-N(38)-C(27)	113.019
4.	H(35)-C(34)-H(36)	108.158
5.	H(35)-C(34)-H(37)	107.499
6.	H(35)-C(34)-N(38)	110.752
7.	H(36)-C(34)-H(37)	107.979
8.	H(36)-C(34)-N(38)	112.760
9.	H(37)-C(34)-N(38)	109.516
10.	H(31)-C(30)-H(32)	108.085
11.	H(31)-C(30)-H(33)	107.841
12.	H(31)-C(30)-N(38)	113.186
13.	H(32)-C(30)-H(33)	107.966
14.	H(32)-C(30)-N(38)	109.908
15.	H(33)-C(30)-N(38)	109.699
16.	C(23)-C(27)-H(28)	109.709
17.	C(23)-C(27)-H(29)	108.644
18.	C(23)-C(27)-N(38)	113.163
19.	H(28)-C(27)-H(29)	106.492
20.	H(28)-C(27)-N(38)	111.238
21.	H(29)-C(27)-N(38)	107.315
22.	C(22)-C(23)-H(25)	107.653
23.	C(22)-C(23)-H(26)	109.682
24.	C(22)-C(23)-C(27)	112.969
25.	H(25)-C(23)-H(26)	106.622
26.	H(25)-C(23)-C(27)	110.408
27.	H(26)-C(23)-C(27)	109.302
28.	C(23)-C(22)-H(24)	107.789
29.	C(23)-C(22)-C(1)	112.948
30.	C(23)-C(22)-C(12)	110.891
31.	H(24)-C(22)-C(1)	106.837
32.	H(24)-C(22)-C(12)	106.832
33.	C(1)-C(22)-C(12)	111.209
34.	C(14)-N(21)-C(12)	118.485
35.	H(20)-C(17)-C(15)	121.538
36.	H(20)-C(17)-C(14)	120.486
37.	C(15)-C(17)-C(14)	117.976
38.	H(19)-C(15)-C(17)	120.726
39.	H(19)-C(15)-C(13)	120.450
40.	C(17)-C(15)-C(13)	118.824
41.	H(18)-C(14)-N(21)	115.955
42.	H(18)-C(14)-C(17)	120.433
43.	N(21)-C(14)-C(17)	123.612
44.	H(16)-C(13)-C(15)	120.691
45.	H(16)-C(13)-C(12)	120.063
46.	C(15)-C(13)-C(12)	119.246
47.	C(22)-C(12)-N(21)	117.243
48.	C(22)-C(12)-C(13)	120.901
49.	N(21)-C(12)-C(13)	121.856
50.	H(10)-C(6)-C(1)	119.323
51.	H(10)-C(6)-C(5)	119.554
52.	C(1)-C(6)-C(5)	121.112
53.	H(9)-C(5)-C(6)	120.409
54.	H(9)-C(5)-C(4)	120.308
55.	C(6)-C(5)-C(4)	119.283
56.	Br(11)-C(4)-C(5)	119.491
57.	Br(11)-C(4)-C(3)	119.511
58.	C(5)-C(4)-C(3)	120.998
59.	H(8)-C(3)-C(4)	120.514
60.	H(8)-C(3)-C(2)	120.582
61.	C(4)-C(3)-C(2)	118.903
62.	H(7)-C(2)-C(3)	118.831
63.	H(7)-C(2)-C(1)	119.659
64.	C(3)-C(2)-C(1)	121.510
65.	C(22)-C(1)-C(6)	121.351
66.	C(22)-C(1)-C(2)	120.455
67.	C(6)-C(1)-C(2)	118.194

The potential energy surface of reported compound has been carried to check any possible existence of conical intersection between the ground and first excited state, however, the DFT based B3LYP/6-311G (d,p) level of computations were not able predict any imaginary frequencies implying that the stationary point is located at the global minimum of the potential energy hyper-surface (Figure 2). The optimized bond lengths, bond angles and dihedral angles were obtained using B3LYP with 6-311G(d,p) level theory. The calculated optimized electronic energies of Brompheniramine is -3304.96 Hartree's with the Zero point energy correction 0.3166 Hartree's,which confirms the molecular stability of the AHC1. The analytical and energies of thermodynamical parameters of Brompheniramine or Dexbrompheniramine maleate with 298.150 K at 1.000 atm pressure reported in Table 1 and the bond distances in Table 2.

3.2. Mulliken electronegativity and APT Charges

The quantum chemical calculations are used to determine electronegativity of pure s, p and d states and atomic partial charges (APT) for the AHC1 compound involves fitting the charges to electrostatic potentials (ESPs) computed with *abinitio* quantum mechanics at sampling points around the reported compounds (Figure 3 and Table 4). Mulliken electronegativity (χ) can be computed as follows: $\chi=(I+A)/2$, where I is ionization energy ($I=-E_{HOMO}$) and A is electron affinity ($A=-E_{LUMO}$). Softness is measure of extent of chemical reactivity $S=1/2\eta$ and harness is measured $\eta=(I-A)/2$. The electrophilicity index $\omega=(-\chi^2/2\eta)$ is a measure of energy lowering due to maximum electron flow between donor and acceptor [27,28].

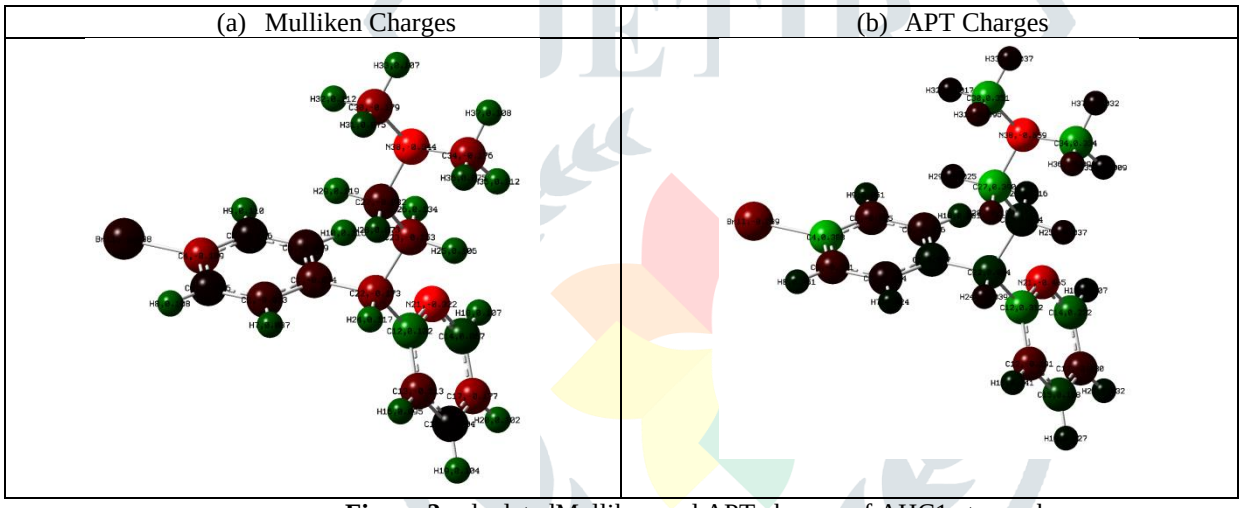

Figure 3.calculatedMulliken and APT charges of AHC1 at gas phase

3.3. Dipole moments

Generally, the dipole moment values of compounds indicate bond polarities and charge densities in molecules. The computed dipole moment of AHC1 compound with B3LYP/6-311G(d,p) level of theory have been reported values is 3.5901 D, which significantly showed that the AHC1 is relatively polarized and more active of Brompheniramine or Dexbrompheniramine maleate [29].

3.4. Molecular Electrostatic Potential (MEP)

The molecular electro-static potential surface of the AHC1 compound has been determined by B3LYP/6-311 G(d,p) method to know the relative polarity of the molecules. The electrostatic potential contour map for positive and negative potentials of title compound is shown in Figure 4. The electron rich or negative charge of the MEP surface is shown in red colour, the blue region exposes the electron deficient or partially positive charge, light blue region shows slightly electron deficient region, the slightly electron rich region is indicated by yellow and the green colour shows neutral [28,29]

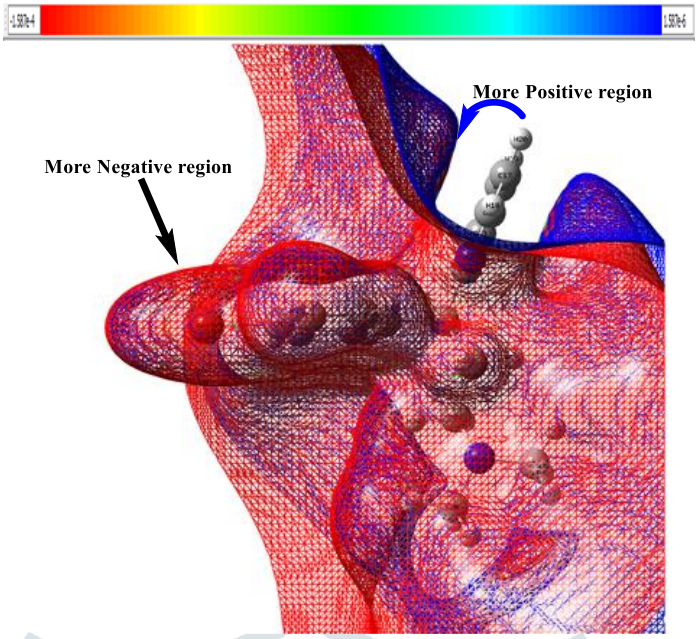

Figure 4. ESP of AHC1 at gas phase

3.5. Analysis of frontier molecular orbitals

The highest occupied molecular orbital and lowest unoccupied molecular orbital are named as frontier molecular orbital (FMOs). A molecular orbital describes the behavior of electrons in a molecule. Electrostatic potential of a molecule is a good tool to assess the molecules reactivity towards positively or negatively charged reactants. The energies of HOMO, LUMO and their orbital energy gap are calculated by using B3LYP/6-311 G(d,p) method. The pictorial structure representation of the frontier molecular orbitals and their respective positive and negative regions are presented in Figure 5. The positive and negative surfaces is shown in red and green colour, respectively. The electron cloud is mainly located on the aromatic ring and is of π type, but in case of LUMO it is π^* in nature, therefore, the HOMO–LUMO transition is $\pi \rightarrow \pi^*$ in nature. The FMOs play crucial role in the optical and electrical properties of molecules. The energy gap between HOMO and LUMO helps to predict the chemical reactivity and kinetic stability of the molecule. A molecule with small energy gap has high chemical reactivity and low kinetic stability [26,27]. The energy gap values clearly show that enol form has higher energy gap than keto form, which reveals the lower chemical reactivity and higher kinetic stability of enol form than keto form. The energy gap (Figure 6) of LUMO-HOMO of AHC1 is 4.727 eV, which clearly indicates the charge transfer interface with in the molecule. The narrow energy gap between HOMO and LUMO facilitates molecule to be NLO active.

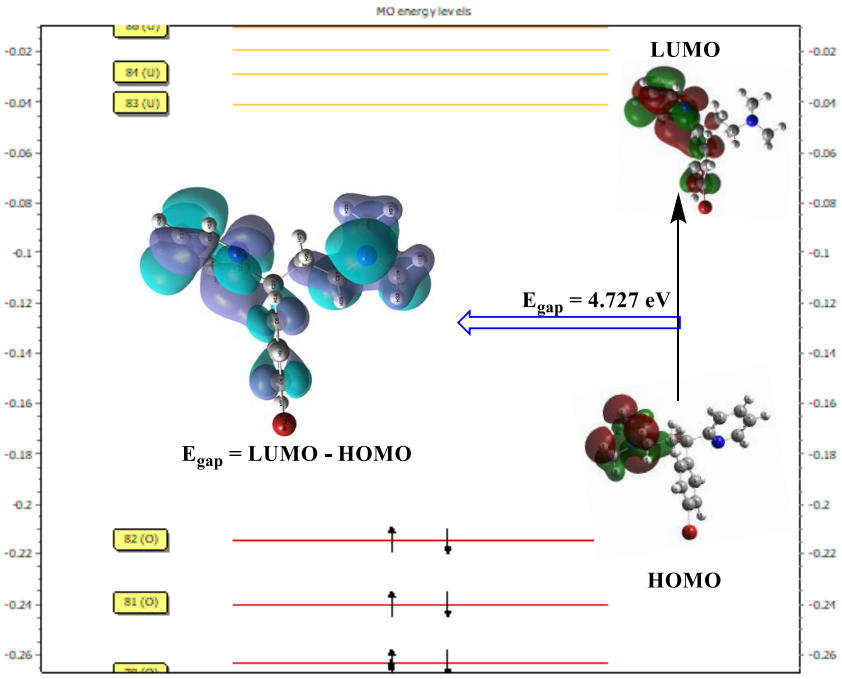

Figure 5. HOMO-LUMO molecular energy level diagram of AHC1 with gas phase

3.6. Electronic Transition

The electronic transitions of the Brompheniramine or Dexbrompheniramine maleate has been explained based on time dependent density functional theory with B3LYP/6-311G(d,p) at gas phase using the optimized geometry of the ground state (Figure 6). AHC1 form Gives intense peak at 261 nm, 272 nm and 293 nm and in the DMSO solvent it forms at 259 nm, 267 nm and 285 nm as high intense peak is assigned to π→π* and n→π* transitions of the conjugated aromatic ring.The most intense electronic transition occurs between the highest occupied molecular orbital to the lowest unoccupied molecular orbital, the energy gap of AHC1 is E_{gap} = 4.727 eV at gas phase <E_{gap} = 4.864 eV at DMSO solvent (Figure 7).

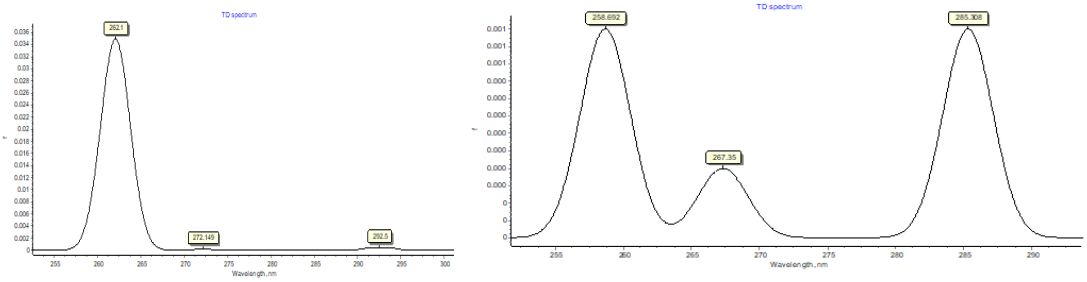

(a) (b)

Figure 6.TD Spectrum of AHC1 (a) at gas phase (b) in DMSO Solvent

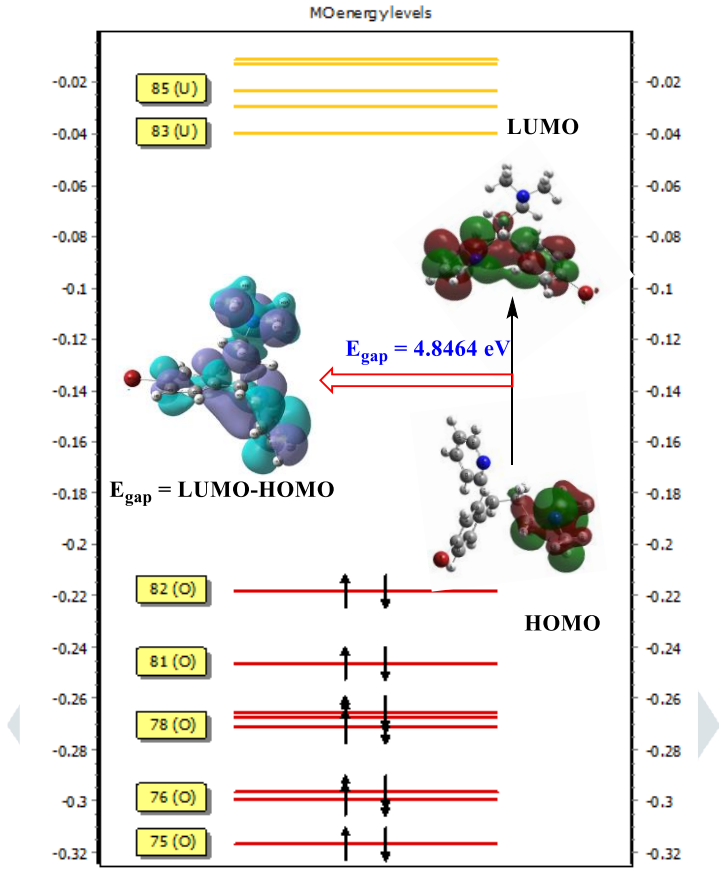

Figure 7. HOMO-LUMO molecular energy level diagram of AHC1 in DMSO solvent

3.7 Computed Vibrational frequencies

Computed IR frequencies shown in Figure 8 with B3LYP/6-311G(d,p) level of theory. In order to determine possible interaction between drug with carrier, vibrational frequencies has been calculated. The AHC1 shows characteristic peak of N-H stretching vibration at 2903 cm^{-1}. The FTIR spectra of optimized formulation showed same peak as that of pure drug AHC1.

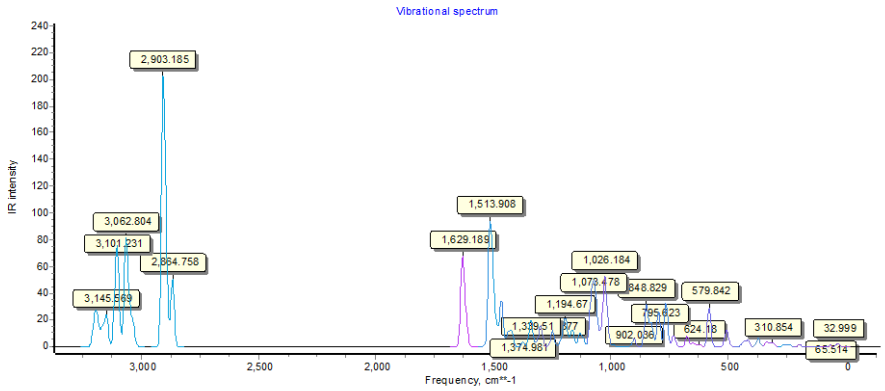

Figure 8. Computed vibrational frequencies of AHC1 at gas phase

Carbon-Carbon stretching band of phenyl group is appeared in range of 1500-800 cm^{-1} and the bands at around 3100 cm^{-1} are due to the aromatic C-H stretching vibration respectively. All other vibrational bands of aromatic C-H stretching, aromatic C=C stretching and C-N stretching are also observed. Further computed vibrational spectra is compared with the computed Raman intensity spectra (Figure 9) which is assigned as in the assignments of vibrational frequencies.

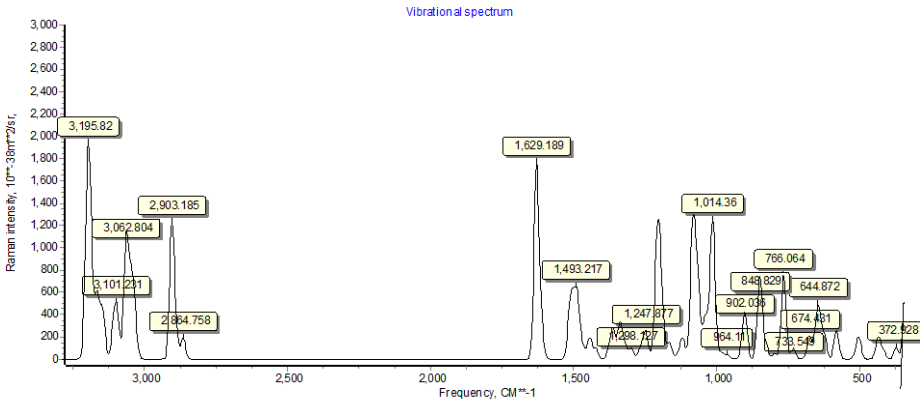

Figure 9. Computed Raman intensity spectrum of AHC1 at gas phase

3.8 NMR Chemical Shifts

The NMR techniques are used to predict presence of particular nuclei in a compound. It helps to elucidate the molecular structural information when the nucleus exposed to electromagnetic radiation in a strong magnetic field [28]. The geometry optimization of Brompheniramine or Dexbrompheniramine maleate were performed at the gradient corrected density functional level of theory using the hybrid B3LYP method based on Becke's three parameters functional of DFT and gauge-including atomic orbital (GIAO) $^{13}C\{^{1}H\}$-NMR chemical shift calculations of the compounds have been computed using B3LYP/6-311G(d,p) basis set [28,29].^{1}H NMR (Figure 10) and ^{13}C-NMR (Figure 11) chemical shifts of the compound ATC1 is given and the N-methyl group's carbon (C30, C34) of the title compound give chemical shielding tensor appears 134.510 and 141.079 ppm at gas phase, 135.265, 143.978 ppm in DMSO solvent which reveals that the downfield of C30 and C34 is due to the influence of adjacent highly polar N- in the solvent.

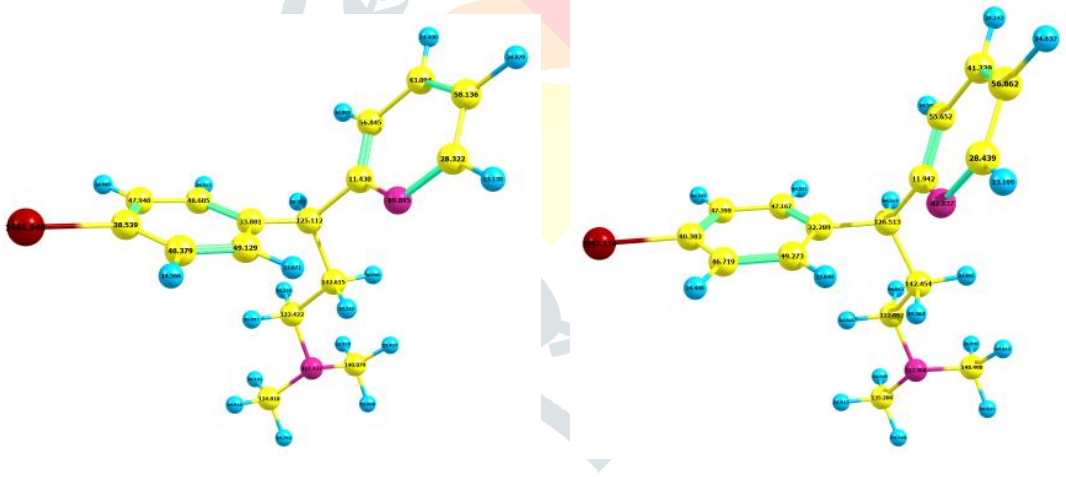

(a) (b)

Figure 10. NMR Shielding tensor values of AHC1 (a) at gas phase (b) in DMSO solvent

On high demand of NMR chemical shielding tensors, definitely DFT studies determines of degree of aromaticity and the NMR chemical shift methodology offers one unique probe of aromaticity based on one defining characteristics of an aromatic system, its ability to sustain a diatropic ring current of the reported moiety's. This leads to a response to an imposed external magnetic field with a strong (negative-red colour contour maps) shielding at the center of the AHC1 [30] about XX axis (Figure 11) and the computed absolute magnetic shielding at pyridine ring centers it shows strong negative shielding at the ring center (negative nucleus-independent chemical shift (NICS)), while anti-aromatic systems reveal positive NICS at the N-methyl center (blue-coloured contour maps in Figure 11).

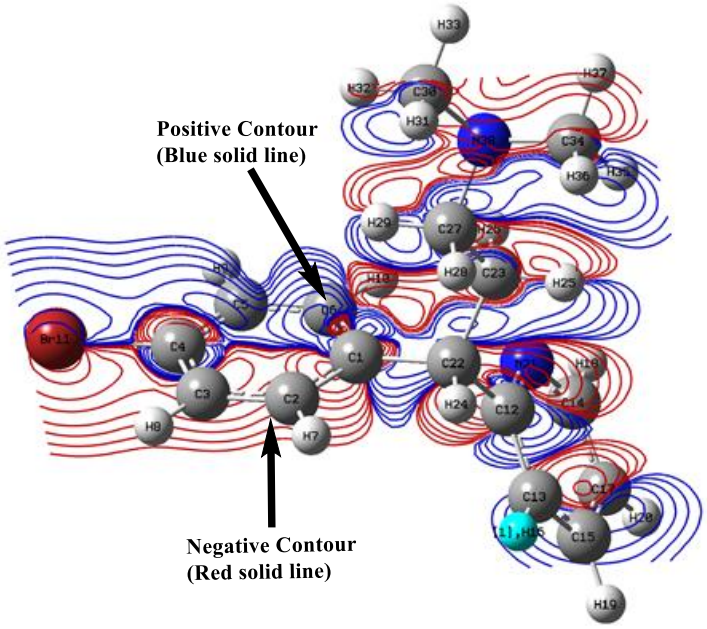

Figure 12. Computed Magnetic shielding tensor about XX axis of AHC1 at gas phase

3.9. Non-linear optical (NLO) properties

The NLO calculations have made an important contribution to the electronic polarization of molecule and structural properties relationship and the NLO response calculation was performed on the optimized geometry using B3LYP/6-311G(d,p) level of theory and the first static hyperpolarizability is a third rank tensor that can be described by a 3×3×3 matrix with 27 components of the 3D matrix can be reduced to 10 components due to the Kleinman symmetry [31-34], i.e., β_{xxx}, β_{xxy}, β_{xyy}, β_{yyy}, β_{xxz}, β_{xyz}, β_{yyz}, β_{xzz}, β_{yzz} and β_{zzz} respectively and the computed first static hyperpolarizability (β) values of these Brompheniramine or Dexbrompheniramine maleate were calculated and converted to electrostatic units (esu) and represented in the Table 9. The calculated first static hyperpolarizability (β) tensors of AHC1 is β_{tot}= 8.1235 x 10^{-30}e.s.u is predicted to have larger NLO property than that of other anti-histamine compounds [35,36].

IV. CONCLUSION

In the present work, the DFT calculations of Brompheniramine or Dexbrompheniramine maleate is carried out using B3LYP/6-311G (d,p) level of theory to evaluate the PES, vibrational frequencies (IR), electronic transition, TD-DFT and NMR shielding tensors (^{13}C and ^{1}H). Further, Mulliken Charges, APT charges, the energies of the frontier molecular orbitals (HOMO/LUMO) with molecular energy level diagram and electrostatic potential surface analysis at gas phase and also in DMSO solvent. In addition, an investigation of molecular first static hyperpolarizability (β_{tot}) were also computed. Dipole moment values showed that the relatively polarized 3.59 Debye. The energy gap of LUMO-HOMO of AHC1 at gas phase and in DMSO solvent are 4.727eV and 4.846 eV respectively, which clearly indicates the charge transfer interface with in the molecule. The narrow energy gap between HOMO and LUMO facilitates molecule to be NLO active.

Acknowledgements:

All the authors sincerely acknowledge the Management, Kongunadu Arts and Science College, Coimbatore-641 029, India for providing us with basic infrastructures to carry out this research.

Author Agreement/Declaration:

This is to certify that all authors have seen and approved the final version of the manuscript being submitted. They warrant that the article is the authors' original work, hasn't received prior publication and isn't under consideration for publication elsewhere.

Declarations of interest:

There is no conflict of interest.

References

[1] Videla, S.; Lahjou, M.; Guibord, P.; Xu, Z.; Tolrà, C.; Encina, G.; Sicard, E.; Sans, A. Food effects on the pharmacokinetics of doxylamine hydrogen succinate 25 mg film-coated tablets: A single-dose, randomized, two-period crossover study in healthy volunteers. Drugs R&D 2012, 12, 217–225.

[2] Bovet, D. Introduction to antihistamine agents and antergan derivatives. Ann. N. Y. Acad. Sci. 1950, 50, 1089–1126. [CrossRef] [PubMed]

[3] Schutte-Rodin, S.; Broch, L.; Buysse, D.; Dorsey, C.; Sateia, M. Clinical guideline for the evaluation and management of chronic insomnia in adults. J. Clin. Sleep Med. 2008, 4, 487–504. [PubMed]

[4] Roth, T.; Rogowski, R.; Hull, S.; Schwartz, H.; Koshorek, G.; Corser, B.; Seiden, D.; Lankford, A. Efficacy and safety of doxepin 1 mg, 3 mg, and 6 mg in adults with primary insomnia. Sleep 2007, 30, 1555–1561. [PubMed]

[5] Church, M.; Maurer, M.; Simons, F.; Bindslev-Jensen, C.; van Cauwenberge, P.; Bousquet, J.; Holgate, S.; Zuberbier, T. Risk of first-generation H1-antihistamines: A GA2LEN position paper. Allergy 2010, 65, 459–466. [CrossRef] [PubMed]

[6] Monti, J.M.; Monti, D. Histamine H1 receptor antagonists in the treatment of insomnia. CNS Drugs 2000, 13, 87–96. [CrossRef]

[7] Chihara, Y.; Sato, A.; Ohtani, M.; Fujimoto, C.; Hayashi, T.; Nishijima, H.; Yagi, M.; Iwasaki, S. The effect of a first-generation H1-antihistamine on postural control: A preliminary study in healthy volunteers. Exp. Brain Res. 2013, 231, 257–266. [CrossRef] [PubMed]

[8] Simon, F.E.R.; Simons, K.J. H1 antihistamines: Current status and future directions. World Allergy Organ. J. 2008, 1, 145–155. [CrossRef]

[9] Wang, J.; Li, Y.; Yang, Y.; Zhang, J.; Du, J.; Zhang, S.; Yang, L. Profiling the interaction mechanism of indole-based derivatives targeting the HIV-1 gp120 receptor. RSC Adv. 2015, 5, 78278–78298. [CrossRef]

[10] Li, P.; Chen, J.; Wang, J.; Zhou, W.; Wang, X.; Li, B.; Tao, W.; Wang, W.; Wang, Y.; Yang, L. Systems pharmacology strategies for drug discovery and combination with applications to cardiovascular diseases. J. Ethnopharmacol. 2014, 151, 93–107. [CrossRef] [PubMed]

[11] Ru, J.; Li, P.; Wang, J.; Zhou, W.; Li, B.; Huang, C.; Li, P.; Guo, Z.; Tao, W.; Yang, Y.; et al. TCMSP: A database of systems pharmacology for drug discovery from herbal medicines. J. Cheminform. 2014, 6, 13. [CrossRef] [PubMed]

[12] Yu, H.; Chen, J.; Xu, X.; Li, Y.; Zhao, H.; Fang, Y.; Li, X.; Zhou, W.; Wang, W.; Wang, Y. A systematic prediction of multiple drug-target interactions from chemical, genomic, and pharmacological data. PLoS ONE 2012, 7, e37608. [CrossRef] [PubMed]

[13] Frisch M.J, Trucks G.W, Schlegel H.B, Scuseria G.E, Robb M.A, Cheeseman J.R, Scalmani G, Barone V, Mennucci B, Petersson G.A, Nakatsuji H, Caricato M, Li X, Hratchian H.P, Izmaylov A.F, Bloino J, Zheng G, Sonnenberg J.L, Hada M, Ehara M, Toyota K, Fukuda R, Hasegawa J, Ishida M, Nakajima T, Honda Y, Kitao O, Nakai H, Vreven T, Montgomery J.A, Peralta Jr, J.E, Ogliaro F, Bearpark M, Heyd J.J, Brothers E, Kudin K.N, Staroverov V.N, Kobayashi R, Normand J, Raghavachari K, Rendell A, Burant J.C, Iyengar S.S, Tomasi J, CossiM,Rega N, Millam J.M, Klene M, Knox J.E, Cross J.B, Bakken V, Adamo C, Jaramillo J, Gomperts R, Stratmann R.E, Yazyev O, Austin A.J, Cammi R, Pomelli C, Ochterski J.W, Martin R.L, Morokuma K, Zakrzewski V.G, Voth G.A, Salvador P, Dannenberg J.J, Dapprich S, Daniels A.D, Farkas O, Foresman J.B, Ortiz J.V, Cioslowski J, Fox D.J. Gaussian 09. Inc, Wallingford: CT, 2009.

[14] Alasalvar C, Soylu M. S, Güder A, Albayrak Ç. D, Apaydın G, Dilek N. Crystal structure, DFT and HF calculations and radical scavenging activities of (E)-4,6-dibromo-3-methoxy-2-[(3-methoxyphenylimino)methyl]phenol. SpectrochimicaActa Part A: Molecular and Biomolecular Spectroscopy 2014; 125: 319–327.

[15] Pouralimardan O, Chamayou A.C, Janiak C, Hosseini-Monfared H. Hydrazone Schiff base-manganese (II) complexes: Synthesis, crystal structure and catalytic reactivity. Inorg. Chim. Acta 2007; 360:1599–1608.

[16] Pandey A.K, Mishra V.N, Singh V. Biological, Electronic, NLO, NBO, TDDFT and vibrational analysis of 1-benzyl-4-formyl-1H-pyrrole-3-carboxamide. Iranian Journal of chemistry and chemical engineering 2018.

[17] Kohn W. Nobel Lecture: Electronic structure of matter-wave functions and density functional. Reviews of Modern Physics 1999; 71:1253-1266.

[18] Becke A. D. Density-functional exchange-energy approximation with correct asymptotic behavior. Physics Review A 1988. 38:3098.

[19] Lee C, Yang W, Parr R.G. Development of the Colle-Salvetti correlation-energy formula into a functional of the electron density. Physics Review B 1988; 37:785.

[20] Frisch M. J, Pople J. A, Binkley J. S. Self- consistent molecular orbital methods 25. Supplementary functions for Gaussian basis sets. J. Chem. Physics1984; 80:3265-3269.

[21] Hehre W. J, Radom L, Schleyer P. V. R, Pople J. A. Ab initio Molecular Orbital Theory. New- York: John Wiley, 1986.

[22] Ditchfield R. Self-consistent perturbation theory of diamagnetism: I. A gauge-invariant LCAO method for N.M.R. chemical shifts. Molecular Physics 1974; 27: 789-807.

[23] Fukui H, Miura K,Shinbori H. Calculation of NMR chemical shifts. VI. Gauge invariant and Hermitian condition. The Journal of Chemical Physics1985; 83: 907-908.

[24] Wolinski K. , Hinton J. F, Pulay P, Efficient implementation of the gauge-independent atomic orbital method for NMR chemical shift calculations, Journal of American Chemical Society 1990; 112: 8251–8260.

[25] Häser M, Ahlrichs R, Baron H. P, Weiss P, Horn H. Direct computation of second-order SCF properties of large molecules on workstation computers with an application to large carbon clusters. Theoretical Chemical Accounts 1992; 83: 455.

[26] Chidangil S, Shukla M.K, Mishra P.C. A molecular electrostatic potential mapping study of some fluoroquinolone anti-bacterial agents. Journal of Molecular Modelling 1998; 4: 250–258.

[27] Dennington II Roy D, Keith Todd A, Millam John M. Gauss View. Version 6.0.16: Semichem, Inc., 2000-2016.

[28] Wang Y, Saebar S, Pittman Jr C.U. The structure of aniline by ab initio studies. Journal of Molecular Structure (Theochem) 1993; 281: 91–98.

[29] Şahin Ö, ÖzmenÖzdemir Ü, Seferoğlu N, KaragözGenc Z, Kaya K, Aydıner B, Tekin S, Seferoğlu Z. New platinum (II) and palladium (II) complexes of coumarin-thiazole Schiff base with a fluorescent chemosensor properties: Synthesis, spectroscopic characterization, X-ray structure determination, in vitro anticancer activity on various human carcinoma cell lines and computational studies. Journal of Photochemistry & Photobiology, B: Biology 2018; 178: 428–439.

[30] Reed A.E, Weinhold F. Natural localized molecular orbitals. Journal of Chemical Physics 1985; 83: 1736–1740.

[31] Reed A.E, Weinstock R.B, Weinhold F. Natural population analysis. Journal of Chemical Physics 1985; 83: 735–746.

[32] Dani V.R. Organic Spectroscopy. New Delhi: Tata McGraw Hill, 1995.

[33] Von Schleyer P, Maerker C. ,Dransfield A, Jiao H, Van Eikema Hommes N. J. R. Nucleus-Independent Chemical Shifts: A Simple and Efficient Aromaticity Probe. Journal of American Chemical Society 1996; 118: 6317.

[34] Parr R.G, Pearson R.G. Absolute hardness: companion parameter to absolute electronegativity. Journal of American Chemical Society 1983; 105: 7512-7516.

[35] Parr R.G, Szentpaly L.V, Liu S. Electrophilicity Index. Journal of American Chemical Society 1999; 121: 1922-1924.

[36] Wright J.S, Carpenter D.J, McKay D.J, Ingold K.U. Theoretical Calculation of Substituent Effects on the O−H Bond Strength of Phenolic Antioxidants Related to Vitamin E. Journal of American Chemical Society 1997; 119: 4245-4252.